Physics and chemistry of interstellar ice

Guss, K.M.R.

Chapter V

HIGHLY RESOLVED INFRARED SPECTRA OF PURE CO_2 ICE

Highly resolved infrared spectra of pure CO_2 ice (15-75 K),
K. Isokoski, C. Poteet, and H. Linnartz, *Astronomy & Astrophysics*, 2013, to be submitted.

Part of *Anomalous CO_2 ice towards HOPS-68: a tracer of protostellar feedback*, C. Poteet, K.M. Pontoppidan, S.T. Megeath, D.M. Watson, K. Isokoski, J.E. Bjorkman, P.D. Sheehan and H. Linnartz, *Astrophysical Journal*, 2013, in press.

Abstract

The ν_2 bending mode of pure CO_2 ice around 15.2 μm exhibits a fine double-peak structure that offers a sensitive probe to study the physical and chemical properties of solid CO_2 in space. Current laboratory spectra do not fully resolve the CO_2 ice features. In order to improve the fitting of the observed CO_2 features, high-resolution solid-state infrared spectra of pure CO_2 ice are recorded in the laboratory for a series of astronomically relevant temperatures and at an unprecedented level of detail. The infrared spectra of pure CO_2 ice are recorded in the 4000 to 400 cm^{-1} (2.5-25 μm) region at a resolution of 0.1 cm^{-1} using Fourier Transform Infrared Spectroscopy. Accurate band positions and band widths (FWHM) of pure CO_2 ice are presented for temperatures of 15, 30, 45, 60 and 75 K. The focus of this spectroscopic work is on the CO_2 (ν_2) bending mode, but more accurate data are also reported for the $^{12}CO_2$ and $^{13}CO_2$ (ν_3) stretching mode, and CO_2 ($\nu_1+\nu_3$) and ($2\nu_2+\nu_3$) combination modes.

5.1 Introduction

Solid carbon dioxide, CO_2, is an important tracer of the chemical and physical history of protostars and their surroundings (Whittet et al. 1998, Ehrenfreund et al. 1998, Gerakines et al. 1999, Boogert et al. 2000, Nummelin et al. 2001, Pontoppidan et al. 2008). It constitutes a significant part of interstellar ice with abundances relative to solid H_2O varying from ~15 to 40 % in quiescent dark clouds (d'Hendecourt & Jourdain de Muizon 1989, Whittet et al. 1998, 2007, 2009, Bergin et al. 2005, Knez et al. 2005) and circumstellar envelopes of low- and high-mass protostars (Gerakines et al. 1999, Nummelin et al. 2001, Boogert et al. 2004, Pontoppidan et al. 2008, Zasowski et al. 2009, Cook et al. 2011). The observed abundances of solid CO_2 are a factor of ~100 higher than in the gas phase (van Dishoeck et al. 1996, Boonman et al. 2003) and cannot be reproduced by gas-phase chemical models (Bergin et al. 1995). The formation of CO_2 is therefore assumed to proceed through reactions in ices on interstellar dust grains.

CO_2 is readily produced in UV photoprocessed CO-H_2O laboratory ice, with an efficiency high enough to be driven by cosmic-ray induced UV field in dense interstellar regions (Watanabe & Kouchi 2002). Comparable CO_2 ice abundances are however observed in regions with and without additional UV photons from a nearby protostar, suggesting a formation route which does not depend on the available UV field. Cosmic-ray processing of pure CO laboratory ice has been also shown to be a viable mechanism for CO_2 production in the ISM (Jamieson et al. 2006), and seems plausible given the large abundances of pure CO ice (Pontoppidan et al. 2003b). A number of other reaction schemes have been proposed and/or studied including non-energetic surface-catalyzed CO oxidation (Tielens & Hagen 1982, Roser et al. 2001); hydrogenation of CO-O_2 binary ice, providing a formation route through the CO-OH intermediate (Ioppolo et al. 2011); and energetic processing (low-energy ion irradiation) of ices containing C- and O-bearing molecules as well as carbon grains covered by water ice (Ioppolo et al. 2009). Recent observational and experimental work suggests that interstellar ices are unlikely to contain significant amounts of CO intimately mixed in H_2O (Pontoppidan et al. 2003b, Cuppen et al. 2011). This is inconsistent with the CO_2 formation mechanisms relying on or resulting in CO in H_2O-rich ices. Cuppen et al. (2011) further demonstrate that the observed CO ice feature is better reproduced by CO mixed in CH_3OH ice. Indeed, CH_3OH is readily produced through CO hydrogenation (Watanabe et al. 2004, 2006, Fuchs et al. 2009) and CO_2 produced in water-poor CO ice should therefore be intimately mixed also with CH_3OH.

The molecular environment in which CO_2 is observed provides, therefore, valuable information on its formation mechanism; CO_2 located in ice dominated by H_2O, CO and/or CH_3OH is a direct hint for a possible chemical connection. The CO_2 (ν_2) bending mode at 15.2 μm (660 cm^{-1}) is particularly sensitive to its molecular environment and has been observed towards a number of sources ranging from luminous young stars (Gerakines et al. 1999, Pontoppidan et al. 2008) to cold, quiescent molecular clouds (Knez et al. 2005, Bergin et al. 2005, Whittet et al. 2007). The appearance of absorption features not only depends on ice composition, but also on ice temperature. In order to characterize different ice environments, the observed CO_2 (ν_2) feature can be decomposed phenomenologically into a finite set of known laboratory ice compositions (Pontoppidan et al. 2008) including pure CO_2 ice. While the profile of the CO_2 feature in each component is fixed, the relative contribution varies from source to source, thus characterizing and quantifying the ices along the line of sights.

A large number of laboratory spectra of solid CO_2 in different molecular environments and for different temperatures are available (Sandford & Allamandola 1990, Ehrenfreund et al. 1997, 1999, van Broekhuizen et al. 2006, White et al. 2009). For most sources, the analysis of the CO_2 (ν_2) feature implies the presence of both hydrogen-rich (H_2O:CO_2) and hydrogen-poor (CO:CO_2) CO_2 ice, as well as CH_3OH containing CO_2 ice (Ehrenfreund et al. 1998), consistent with several of the proposed formation schemes. Most sources also exhibit some contribution from pure CO_2 ice. The occurrence of pure CO_2 is considered to be a result of thermal processing, which causes segregation and/or distillation of mixed components with different volatility (Ehrenfreund et al. 1998, Öberg et al. 2009a, Fayolle et al. 2011). Distillation of CO-rich ice happens at 20-30 K (Pontoppidan et al. 2008). In the laboratory, segregation from H_2O-rich ice requires strong (>100 K) heating (Gerakines et al. 1999), but is lowered to 30 K in the ISM due to longer time scales (Öberg et al. 2009a).

Low-temperature (<20 K) H_2O- and CO-rich ices are characterized by a broad single-peaked CO_2 (ν_2) feature, whereas pure CO_2 produces a double-peaked substructure (Ehrenfreund et al. 1997, van Broekhuizen et al. 2006). In a pure CO_2 lattice the axial symmetry of the linear molecule is broken, giving rise to the so-called Davydov splitting (Davydov 1962, Tso & Lee 1985). The splitting makes the CO_2 bending mode a sensitive probe for the changes in its environment. Prior to this work, the available laboratory spectra of pure CO_2 ice (Sandford & Allamandola 1990, Hudgins et al. 1993, Ehrenfreund et al. 1997, Baratta & Palumbo 1998) were recorded at resolutions of 1–2 cm^{-1}, too low to fully resolve the CO_2 (ν_2) bending mode. van Broekhuizen et al. (2006) recorded CO_2 ice spectra at 15-90 K with 0.5 cm^{-1} resolution but the low S/N ratio prohibit accurate comparison with astronomical data. Particularly for sources with a prominent double-peak structure, such as HOPS-68 (Poteet et al. 2011, Poteet et al. 2013, ApJ, Submitted), the spectral quality of the used pure CO_2 component is important. Using a pure CO_2 component with a properly resolved Davydov splitting can help to avoid overestimation and misinterpretation of the underlying broader features. Ehrenfreund et al. (1997) does not make available the entire temperature series for pure CO_2 ice. Here we have a complete, high-resolution temperature series. In addition to the 15.2 μm bending mode, the resolution of the previous data is not sufficient when studying the narrow $^{13}CO_2$ ice band or the narrow ($\nu_1 + \nu_3$) combination band. These bands will be assessable with the James Webb Space Telescope. Thus, the high-resolution CO_2 laboratory spectra will be needed here as well.

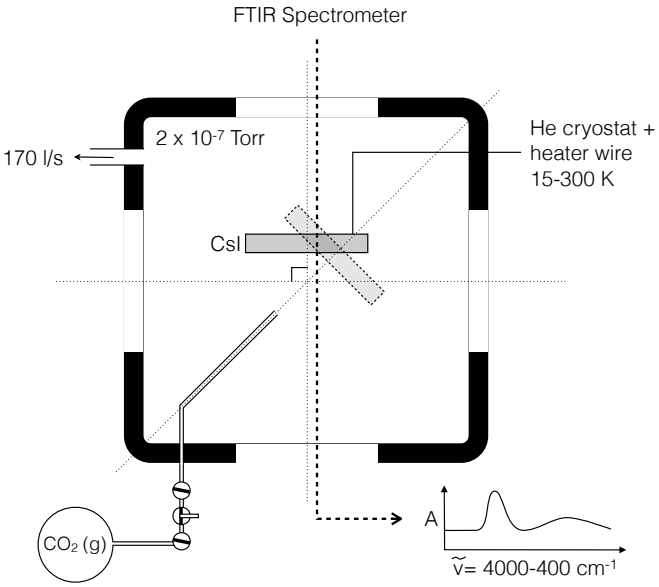

Figure 5.1 – Schematic drawing of the experimental setup for preparation and spectroscopic characterization of the cryogenic CO_2 samples.

5.2 Experimental procedure

The experiments are performed in a high-vacuum (HV) setup first described by Gerakines et al. (1995) (Fig. 5.1). A stainless steel chamber is evacuated by a turbomolecular pump (170 l s^{-1}; Pfeiffer TPH 170) and a rotary vane pump (6 m^3 hr^{-1}; Edwards E2M8) separated by an oil mist filter, allowing a base pressure of 2×10^{-7} Torr at room temperature. The chamber houses a CsI (Caesium Iodide) sample substrate that is cooled down to 15 K by a closed cycle helium cryostat (ADP DE-202). The substrate temperature is controlled between 15 and 300 K, with a precision of 0.1 K, by a resistive heater element and a silicon diode sensor using an external temperature control unit (LakeShore 330). CO_2 (Praxair, 99.998 % purity) is introduced into the system from a gas bulb at 10 mbar filled in a separate vacuum manifold (base pressure $\sim 10^{-5}$ mbar). CO_2 ices are grown onto the substrate at 15 K via effusive dosing of the gaseous sample through a stainless steel capillary along the surface normal. The approximate growth rate is determined by setting the exposure to $\sim 10^{16}$ molecules cm^{-2} s^{-1}. Assuming a monolayer surface coverage of 10^{15} molecules cm^{-2} and a sticking probability of 1, this results in a growth rate of 10 L s^{-1} [1]. Ices are deposited for 5 min resulting in approxmately ~3000 ML. The exact thickness of the samples is derived from the IR band strengths (Sect. 7.5).

The ices are heated from 15 K to 30, 45, 60, 75 and 90 K at a rate of 2 K min^{-1} and allowed to relax for 5 min before recording the absorption spectra. A Fourier Transform InfraRed (FTIR) spectrometer (Varian 670-IR) is used to record the ice spectra in transmission mode from 4000

[1] 1 L (Langmuir) = 1×10^{-6} Torr s ≈ 1 ML

to 400 cm^{-1} (2.5–25 μm) with a spectral resolution of 0.1 cm^{-1}, averaging a total of 256 scans to increase the S/N ratio. Background spectra are acquired at 15 K prior to deposition and subtracted from the recorded ice spectra. The spectra recorded at different temperatures correspond to different ice samples prepared under identical conditions. This procedure is used to minimize the contamination of samples during the relatively long acquisition time (~2 h).

5.3 Results

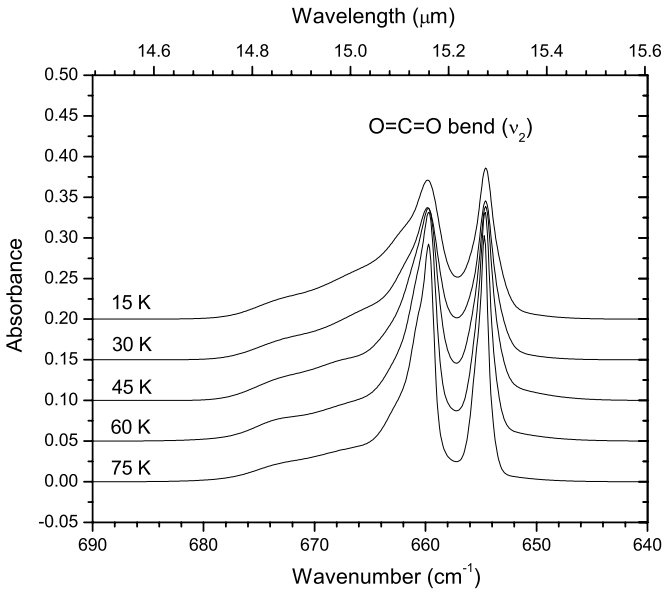

Figure 5.2 – High-resolution (0.1 cm^{-1}) solid-state IR spectra of pure CO_2 ice at 15–75 K showing the $^{12}CO_2$ (ν_2) bending mode. The displayed spectra are obtained by smoothing through superposition of Gaussians.

Figs. 5.2–5.5 show the high-resolution (0.1 cm^{-1}) FTIR spectra of CO_2 ice at 15, 30, 45, 60 and 75 K. Fig. 5.2 shows the spectral region around the ν_2 bending mode (680–645 cm^{-1}). Figs. 5.3 and 5.4 show the CO_2 (ν_3) asymmetric stretching fundamental, for ^{12}C and ^{13}C isotopologue (in natural abundance), respectively. Fig. 5.5 shows the two CO_2 combination bands ($\nu_1 + \nu_3$) and ($2\nu_2 + \nu_3$).

The CO_2 bending fundamental (ν_2) has a double-peaked substructure at ~660/655 cm^{-1}. The high-frequency component is highly asymmetric with a long blue (high wavenumber) wing, while the low-frequency component is relatively symmetric. The $^{12}CO_2$ asymmetric stretching fundamental (ν_3) is located at ~2345 cm^{-1} (4.26 μm), and is redshifted from the gas-phase value 2348 cm^{-1} due to interactions with the surrounding matrix environment. The profile is asymmetric with a prominent blue shoulder and a weaker red (low wavenumber) shoulder. The asymmetric stretching fundamental (ν_3) of the $^{13}CO_2$ isotopologue is found in its natural abundance at ~2283 cm^{-1} (4.38 μm), similarly redshifted from its gas-phase value. $^{13}CO_2$ (ν_3) also exhibits shoulders on both sides. The

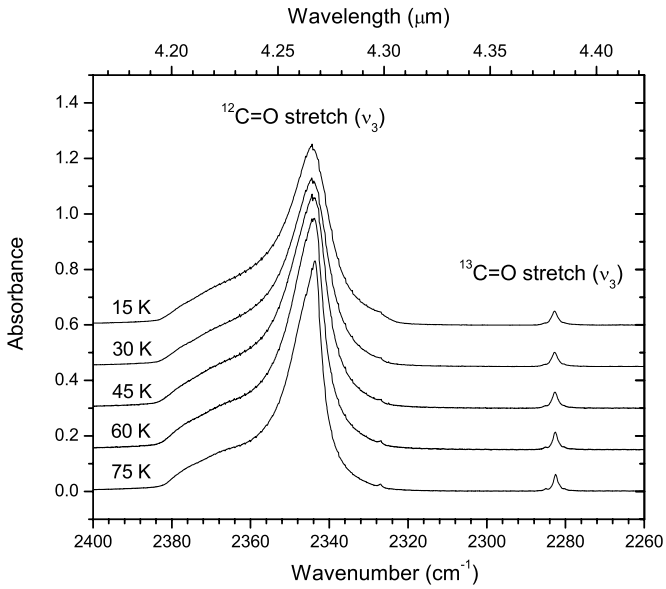

Figure 5.3 – High-resolution (0.1 cm^{-1}) solid-state IR spectra of pure CO_2 ice at 15–75 K showing the $^{12}CO_2$ and $^{13}CO_2$ (ν_3) stretching modes. The zoom-in of the latter is shown in Fig.5.4 The displayed spectra are baseline corrected. Gaseous CO_2 absorption features have been subtracted.

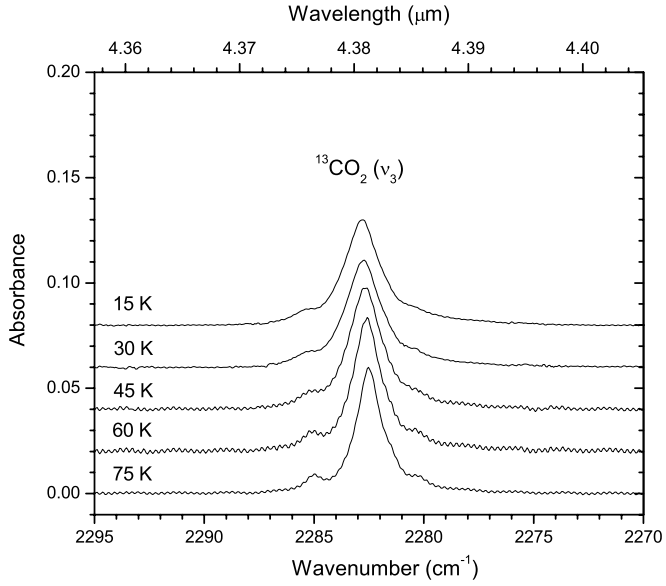

Figure 5.4 – High-resolution (0.1 cm^{-1}) solid-state IR spectra of pure CO_2 ice at 15–75 K showing the $^{13}CO_2$ (ν_3) stretching mode. The displayed spectra are baseline corrected.

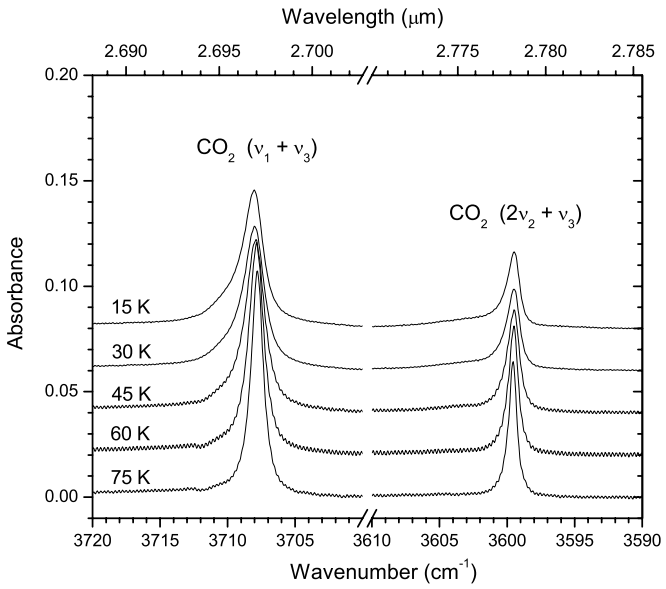

Figure 5.5 – High-resolution (0.1 cm^{-1}) solid-state IR spectra of pure CO_2 ice at 15–75 K showing the ($\nu_1 + \nu_3$) and ($2\nu_2 + \nu_3$) combination modes. The displayed spectra are baseline corrected.

CO_2 (ν_1) symmetric stretching fundamental at ~1385 cm^{-1} (7.22 μm) is IR inactive (Falk & Seto 1986). The CO_2 ($\nu_1 + \nu_3$) combination band and ($2\nu_2 + \nu_3$) combination/overtone bands appear at ~3708 cm^{-1} (2.70 μm) and 3599 cm^{-1} (2.78 μm), respectively. The combination modes have narrow, relatively symmetric profiles. These bands are close to the broad H_2O stretching mode around 3300 cm^{-1} (3.03 μm) which typically dominates the observational ice spectra. However, unlike the strong ν_2 and ν_3 modes, the CO_2 combination and the $^{13}CO_2$ (ν_3) modes are weak and unaffected by grain shape effects. Thus, their band shape profiles depend only on the chemical composition of interstellar CO_2 ice (*e.g.*, Keane et al. 2001).

5.3.1 Corrections

In the laboratory, the CO_2 ice feature around 2350 cm^{-1} is easily contaminated with absorptions of gaseous CO_2 along the IR beam path. Variable concentrations relative to the background spectrum may cause under- or over-subtraction of interfering rotational lines. Same is true for the CO_2 bending mode around 660 $cm^{-1}$where an absorption line is seen around 668 cm^{-1}. The spectra are corrected using a gaseous CO_2 spectrum extracted from the background spectrum (Fig. 5.6). The bending mode region also suffers from spectral artifacts due to being located in the edge of the spectrometer spectral range. The (ν_2) bands presented here are therefore smoothed by superposition of several Gaussians. All spectra have been baseline corrected, and are available in reduced as well as in raw format in the Leiden ice database at `http://www.strw.leidenuniv.nl/lab/databases/co2_hires/`.

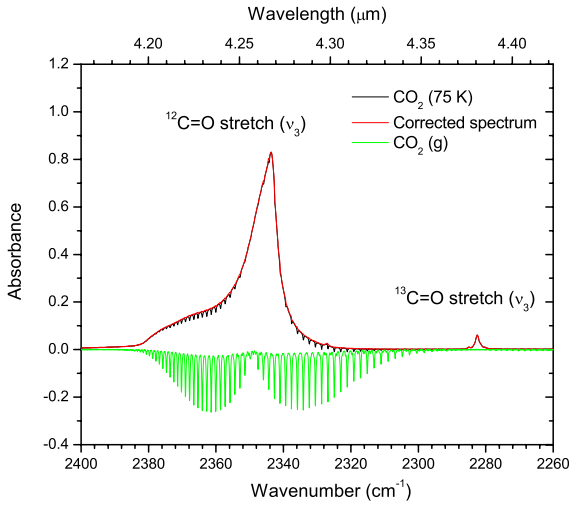

Figure 5.6 – Spectral corrections performed on the CO_2 (ν_3) mode. Rotational fine-structure of gaseous CO_2 (green trace), overlapping with the CO_2 (ν_3) ice band, is subtracted from the raw spectrum (black trace). The corrected spectrum is shown in red.

5.4 Discussion

Table 5.1 lists the band positions and bandwidths of pure CO_2 ice features for the five different temperatures in the 0.1 cm^{-1} resolution spectra. The values are obtained by the integration procedure in the Origin 7.5 software package. Fig. 5.7 visualizes the derived values, including relative peak intensity and integrated area, as a function of temperature, together with other values available from the literature. The values are normalized to those in 0.1 cm^{-1} spectra at 15 K. The influence of thermal annealing on the peak position depends on the influence of the trapping site on the specific vibrational mode. In general, all CO_2 band widths decrease at elevated temperatures. The narrowing is gradual and is observed already between 15 and 30 K. During the thermal annealing process, molecules rearrange themselves by finding energetically more favorable orientations. As the range of environments is reduced, the band profiles become more narrow. Simultaneously, the peak intensities increase. The integrated area of all features peak around 40 K, after which they decline until the ice desorbs between 80 and 90 K.

Comparison of the peak positions in the high-resolution spectra with those from lower resolution studies (Sandford & Allamandola 1990, Ehrenfreund et al. 1997, van Broekhuizen et al. 2006) generally shows agreement within the limitations due to resolution, assuming that at 1 cm^{-1} resolution, the error in position is 0.5 cm^{-1}. At 15 K, the CO_2 (ν_2) bending mode peaks at 659.7 and 654.5 cm^{-1}. The low-wavenumber component shifts by 0.2 cm^{-1} between 45 and 75 K. The observed shift is below the resolution of previous studies. The high-wavenumber component does not shift with temperature. The CO_2 (ν_3) stretching mode, peaking at 2344.4 cm^{-1}in the 15 K spectrum, red-shifts by 0.7 cm^{-1} for temperatures greater than 30 K. The $^{13}CO_2$ stretching mode undergoes a smaller (0.3 cm^{-1}) red-shift in a similar temperature range. The peak positions derived for the combination modes ($\nu_1 + \nu_3$) and ($2\nu_2 + \nu_3$) at 15 K are 3708.0 and 3599.5 cm^{-1}. The position of the combination

Table 5.1 – High-resolution (0.1 cm^{-1}) band positions ($\tilde{\nu}$) and linewidths (FWHM) in pure CO_2 ice.

T	$\tilde{\nu}$	$FWHM$	$\tilde{\nu}$	$FWHM$
(K)	(cm^{-1})	(cm^{-1})	(cm^{-1})	(cm^{-1})
	CO_2 bend (ν_2)			
15	659.72	5.12	654.53	2.09
30	659.78	4.35	654.53	2.00
45	659.72	3.64	654.53	1.86
60	659.78	2.81	654.59	1.48
75	659.72	2.31	654.65	1.17
	$^{12}CO_2$ stretch (ν_3)		$^{13}CO_2$ stretch (ν_3)	
15	2344.41	13.39	2282.76	1.94
30	2344.41	12.88	2282.70	1.91
45	2344.35	11.94	2282.58	1.83
60	2343.81	10.57	2282.58	1.55
75	2343.69	9.23	2282.52	1.38
	CO_2 comb. ($\nu_1 + \nu_3$)		CO_2 comb. ($2\nu_2 + \nu_3$)	
15	3708.02	1.92	3599.48	1.17
30	3708.02	1.91	3599.48	1.21
45	3707.90	1.73	3599.48	1.09
60	3707.84	1.32	3599.48	0.89
75	3707.78	1.10	3599.54	0.74

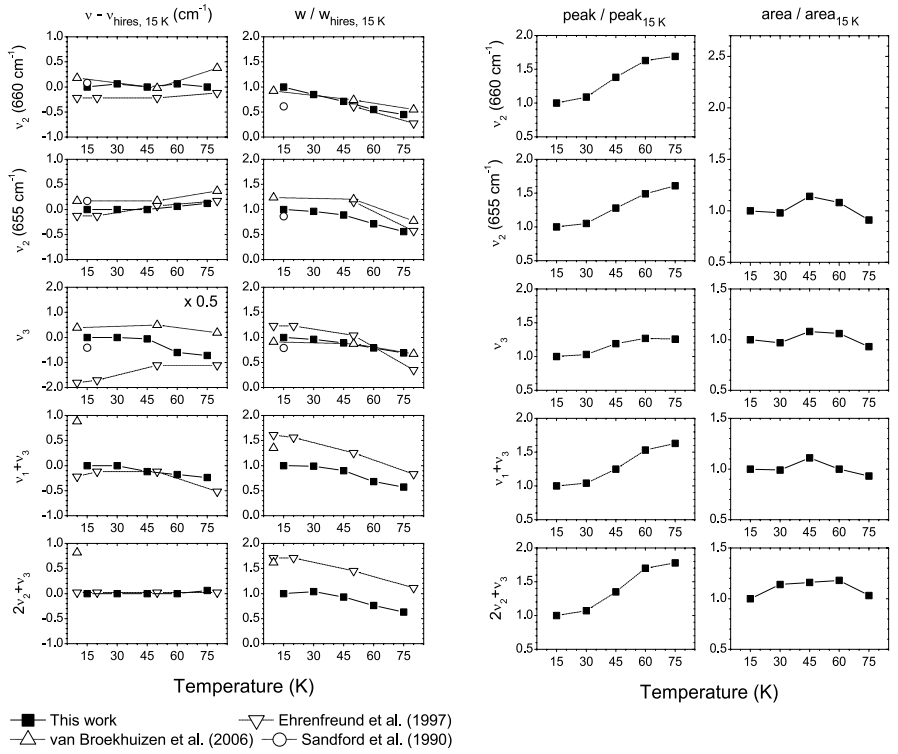

Figure 5.7 – Relative peak position (in cm^{-1}), width, peak intensity and integrated area of the CO_2 ice features as a function of temperature.

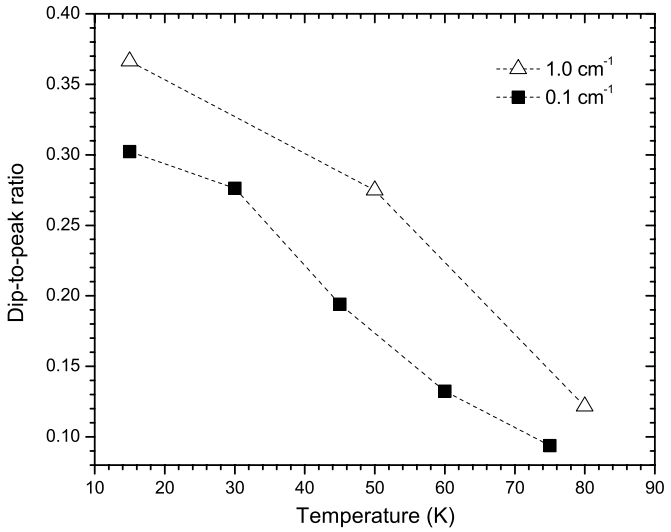

Figure 5.8 – Dip-to-peak ratio at different temperatures derived from the 0.1 cm^{-1} (filled squares) and 1.0 cm^{-1} (open triangles) resolution spectra of the CO_2 bending mode.

modes shifts <0.5 cm^{-1} between 15 and 75 K. The shift of the (ν_1 + ν_3) band occurs after 30 K, towards lower wavenumbers. For the ($2\nu_2$ + ν_3) band a red-shift is observed after a temperature of 60 K is reached.

The main objective of this high-resolution study is to fully resolve the Davydov splitting in the CO_2 (ν_2) bending mode. Fig. 5.8 shows the dip-to-peak ratio, defined by Zasowski et al. (2009) as the local minimum to local maximum ratio of the blue peak, for 0.1 and 1.0 cm^{-1} resolution spectra as a function of temperature. For the high-resolution CO_2 ice feature, the dip-to-peak ratio decreases from 0.3 to <0.10 between 15 and 75 K. The ratio derived from the lower resolution spectra (Ehrenfreund et al. 1997) is ∼20 % larger for all studied temperatures. A smaller dip-to-peak ratio indicates that the CO_2 bending mode and in particular the Davydov split is better resolved in the 0.1 cm^{-1} spectra.

The double peaked structure of the CO_2 bending mode is a diagnostic for the observed 15.2 μm CO_2 ice band. The interpretation of the CO_2 ice composition from observational spectra relies on laboratory spectra of CO_2 for different ice environments (Gerakines et al. 1999, Keane et al. 2001, Pontoppidan et al. 2008). The quality of the laboratory spectra therefore directly influences the derived ice composition from observations. Particularly for sources with larger contributions from pure CO_2 ice, a properly resolved Davydov splitting is a prerequisite for an accurate interpretation. Thus, the incorporation of 0.1 cm^{-1} resolution laboratory spectra (Table 5.1) into the fitting procedure will improve the interpretation of the astronomical observations.

In order to compare with astronomical observations, the thickness of the ice samples has to be known accurately. We derive the ice thickness from the infrared band strengths using eq. 5.1:

Table 5.2 – Thickness of the CO_2 ice samples as derived from different vibrational modes.

T	$\int A\, d\tilde{\nu}$	d	$\int A\, d\tilde{\nu}$	d	$\int A\, d\tilde{\nu}$	d	$\int A\, d\tilde{\nu}$	d
(K)	[cm^{-1}]	[μm]	[cm^{-1}]	[μm]	[cm^{-1}]	[μm]	[cm^{-1}]	[μm]
	CO_2 bend (ν_2)		$^{12}CO_2$ (ν_3)		CO_2 ($\nu_1 + \nu_3$)		CO_2 ($2\nu_2 + \nu_3$)	
15	1.798	0.208	13.460	0.226	0.256	0.233	0.089	0.253
30	1.756	0.204	13.087	0.220	0.253	0.230	0.102	0.290
45	2.055	0.238	14.502	0.243	0.283	0.258	0.103	0.293
60	1.945	0.226	14.280	0.240	0.255	0.232	0.105	0.299
75	1.639	0.190	12.578	0.211	0.237	0.216	0.092	0.260

$$N = \frac{\int \tau\,(\tilde{\nu})\, d\tilde{\nu}}{A_i} = \frac{\ln 10 \int A\,(\tilde{\nu})\, d\tilde{\nu}}{A_i}, \tag{5.1}$$

where N is the column density of the absorbing molecules (in cm^{-2}), $\tau = \ln 10\, A$ is the optical depth, $\int A\,(\tilde{\nu})$ is the integrated absorbance and A_i the intrinsic band strength of a given absorption band. Using the intrinsic band strengths from Gerakines et al. (1995) and Yamada & Person (1964), the derived thickness and integrated absorbance for the CO_2 ice bands are listed in Table 5.2. The thickness is calculated from the column density assuming a monolayer coverage of 1×10^{15} molecules cm^{-2} and a monolayer thickness of 5.54 Å, the lattice constant for solid CO_2 (Keesom & Köhler 1934). These dimensional values are subject to variation in ice morphology, which changes with temperature and likely the ice growth method (Isokoski et al. 2013, A&A, in prep.). Moreover, the intrinsic band strengths reported for CO_2 ice at 14 K are assumed to be applicable for higher temperatures. The increase in thickness for higher temperatures is due to this approximation.

5.5 Optical Constants and Grain Shape-Corrections

The absorption profiles of strong interstellar ice bands are significantly affected by the shape and size of the absorbing particles. Grain shape effects originate from the polarization of interstellar dust by electromagnetic radiation, which produces an induced electric field on the grain surface. The strength of the induced field depends on both the complex dielectric constant of the particular particle and its shape (e.g., Bohren & Huffman 1983, Tielens et al. 1991). Thus, in order to allow for a realistic comparison to astronomical spectra, the absorption profiles of laboratory spectra must first be corrected for size and shape effects. However, such corrections require an accurate determination of the complex refractive index ($n + ik$) of the absorbing species. In this section, we provide a brief comparison between the pure CO_2 ice optical constants from Poteet et al. (2013, ApJ, Submitted) and those derived from the previous lower resolution study by Ehrenfreund et al. (1997). For this comparison, we examine the ν_2 bending mode only.

The real, n, and imaginary, k, parts of the complex refractive index are calculated, using a Kramers-Kronig analysis, from the high-resolution (0.1 cm^{-1}) and lower resolution (1 cm^{-1}) pure CO_2 absorption spectra, following the method previously described in Poteet et al. (2013, ApJ, submitted).

Similar to this study, a thickness of 520 monolayers (or 0.29 μm) is estimated for the 10 K ice sample from Ehrenfreund et al. (1997), using the known absorption band strength of pure CO_2 ice (Eq. 5.1). A comparison of the optical constants for the high-resolution CO_2 bending mode with those derived from the lower resolution absorption spectrum is presented in Fig. 5.9. Differences between the optical constants at these resolving powers are apparent. In particular, the high-resolution refractive index exhibits additional substructure near 653 cm^{-1} that is not resolved in the lower resolution data from Ehrenfreund et al. (1997). For the imaginary part of the refractive index, differences in band width of the high-wavenumber component of the bending mode are found at the different resolving powers. Because the optical constants are consistently derived in the same manner and only a small variation in ice thickness is expected, the dissimilarities between the high- and lower-resolution optical constants are thought to be due to differences in the laboratory instrumental resolving power.

To directly compare the band shape profiles of laboratory-derived spectra to those of astronomical spectra, optical constants must be converted to an opacity. Assuming that an ensemble of interstellar grain shapes can be simulated using a continuous distribution of ellipsoids (CDE; all particle shapes are equally probable), the volume attenuation coefficient, $<C_{abs}>/V$, is calculated in the Rayleigh limit (15 μm$\gg 2\pi a$, where a is the radius of the largest grains) for the ν_2 bending mode (Bohren & Huffman 1983). (For a more thorough discussion on grain shape effects, the reader is referred to Poteet et al. (2013, ApJ, Submitted).) A comparison between the 0.1 and 1 cm^{-1} resolution shape-corrected spectra is shown in Fig. 5.10. We find that the strength of the double-peaked profile is nearly invariable at the different resolving powers. However, similar to the imaginary part of the refractive index, we find that the band width of the high-wavenumber component of the 1 cm^{-1} resolution spectrum is narrower than that of the high-resolution spectrum. This variation is not expected to be due to the small difference in laboratory temperature, but may be a consequence of lower instrumental resolving power.

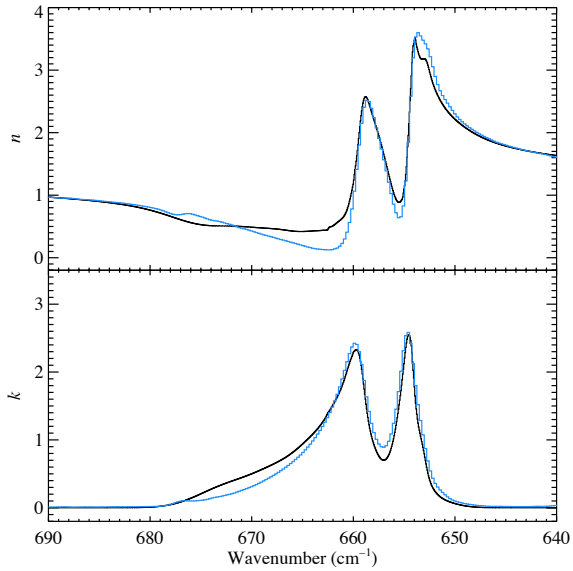

Figure 5.9 – High-resolution (black lines) and lower resolution (blue lines) optical constants for the ν_2 bending mode of pure CO_2 ice. The optical constants are derived using the 0.1 cm^{-1} absorption spectrum (T = 15 K) and 1 cm^{-1} absorption spectrum (T = 10 K) from Ehrenfreund et al. (1997).

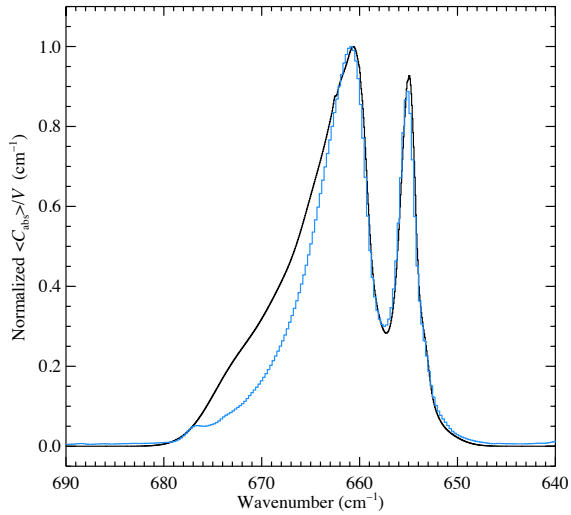

Figure 5.10 – The normalized volume attenuation coefficient (<C_{abs}>/V) for the ν_2 bending mode of pure CO_2 ice. Grain shape-corrections are derived from the 0.1 cm^{-1} optical constants (T = 15 K; black line) and 1 cm^{-1} optical constants (T = 10 K; blue line) from Ehrenfreund et al. (1997), using a continuous distribution of ellipsoids (CDE) in the Rayleigh limit (Bohren & Huffman 1983).

5.6 Summary

In this work we provide highly resolved (0.1 cm^{-1}) IR spectra of pure CO_2 ice at a spectral range of 4000-400 cm^{-1}, at temperatures 15, 30, 45, 60, 75 K. The spectral range covers the fundamental bending mode (ν_2), antisymmetric $^{12}CO_2$ and $^{13}CO_2$ stretching modes (ν_3) and the combination mode ($\nu_1 + \nu_3$) and combination/overtone mode ($2\nu_2 + \nu_3$). The improved spectral parameters are needed for a more accurate interpretation of astronomical ice data. Moreover, the high spectral resolution allows an accurate quantification of thermally induced changes in CO_2 band profiles that are below the resolution of previous work. This is particularly true for shifts in line position below 0.5 cm^{-1}. Also, the Davydov splitting in the ν_2 band is characterized more accurately and allows a better interpretation of astronomical spectra along lines of sight with thermally processed ices, where segregation and/or distillation causes CO_2 to be present in pure form as well. All data are available in the Leiden ice database at:
`http://www.strw.leidenuniv.nl/lab/databases/co2_hires/`.